Growth and Structure of Self-assembled Monolayers of a TTF Derivative on Au(111)

Christian Urban,[†] David Écija,[†] Yang Wang,[‡] Marta Trelka,[†] Iulian Preda,[§] Antje Vollmer,[∥] Nicolás Lorente,[⊥] Andrés Arnau,[#,▽] Manuel Alcamí,[‡] Leonardo Soriano,[§] Nazario Martín,[○,◆] Fernando Martín,[‡] Roberto Otero,[†,◆] José M. Gallego,*[,¶] and Rodolfo Miranda[†,◆]

Departamento de Física de la Materia Condensada, Departamento de Química, and Departamento de Física Aplicada and Instituto de Ciencia de Materiales Nicolás Cabrera, Universidad Autónoma de Madrid, Cantoblanco, 28049 - Madrid, Spain, BESSY, Albert Einstein Strasse 15, D-12489 Berlin, Germany, Centre d'Investigació en Nanociència i Nanotecnologia (CSIC-ICN), Campus de la UAB, Bellaterra, Spain, Departamento de Física de Materiales UPV/EHU and Centro de Física de Materiales CFM−MPC, Centro Mixto CSIC-UPVE/EHU, San Sebastián, Spain, Donostia International Physics Centre (DIPC), Manuel de Lardizabal 4, San Sebastián, Spain, Departamento de Química Orgánica, Universidad Complutense de Madrid, 28040 - Madrid, Spain, Instituto Madrileño de Estudios Avanzados en Nanociencia (IMDEA Nanociencia), Cantoblanco, 28049 - Madrid, Spain, and Instituto de Ciencia de Materiales de Madrid - CSIC, Cantoblanco, 28049 - Madrid, Spain

Received: December 15, 2009; Revised Manuscript Received: February 23, 2010

The adsorption of a TTF derivative (2-[9-(1,3-dithiol-2-ylidene)anthracen-10(9H)-ylidene]-1,3-dithiole, exTTF) on Au(111) has been studied by a combination of scanning tunneling microscopy, photoelectron spectroscopy, and theoretical calculations. The results indicate that the molecule−substrate interaction is dominated by the S−Au bonds. However, due to conformational reasons, only one of the two dithiole rings is in close contact with the surface. As a consequence, the interaction with the Au surface is much smaller (less than half) the interaction of TTF with Au(111), where the four sulfur atoms are in direct contact.

Introduction

One of the motivations behind the increasing number of studies about organic molecules on solid surfaces is the expectation that a thorough understanding of the factors determining the morphology and crystalline structure of thin organic films improves the control over their electronic properties,[1,2] since the energy-level alignment at the organic/metal interface is strongly dependent on the details of the atomic structure.[3,4] This ability would thus facilitate the way for the fast developing field of molecular electronics, which already includes the fabrication of organic displays, thin film transistors, and photovoltaic devices.[5−7]

In particular, in the subfield of organic photovoltaics, the so-called bulk heterojunction solar cells[8,9] are one of the most promising candidates for near-future development. In these cells, the active layer is composed of a blend of donor/acceptor molecules, and since their performance has been shown to depend on the phase separation scale of the blend[10] several attempts have been made to control the morphology of the film from the first layer structure.[11−13] Very recently, it has been shown that mixed thin films of 2-[9-(1,3-dithiol-2-ylidene)anthracen-10(9H)-ylidene]-1,3-dithiole (from now on, exTTF) and phenyl-C61-butyric acid methyl ester (PCBM), deposited on a Au(111) surface in ultrahigh vacuum conditions, spontaneously segregate into a lateral superlattice of interdigitated nanoscale stripes with a characteristic width of about 10−20 nm,[11] a morphology that has been predicted to optimize the efficiency of this type of organic solar cells.[14,15] Since phase separation at

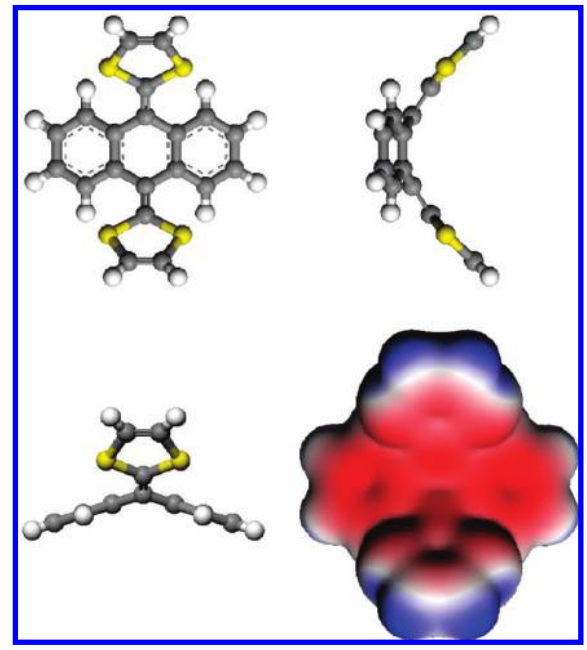

Figure 1. Top, front, and side views of the gas-phase conformation of exTTF (gray, C; white, H; yellow, S). Also shown is a 3D mapped isosurface, a constant charge density surface colored according to the value of the electrostatic potential, which goes from more negative (red) to more positive (blue).

* To whom correspondence should be addressed. E-mail: josemaria.gallego@uam.es.
[†] Universidad Autónoma de Madrid, Departamento de Física de la Materia Condensada.
[‡] Universidad Autónoma de Madrid, Departamento de Química.
[§] Universidad Autónoma de Madrid, Departamento de Física Aplicada.
[∥] BESSY.
[⊥] CSIC-ICN.
[#] Centro Mixto CSIC-UPVE/EHU.
[▽] DIPC.
[○] Universidad Complutense de Madrid.
◆ IMDEA NanoScience.
[¶] Instituto de Ciencia de Materiales de Madrid - CSIC.

10.1021/jp911839b
Published on Web 03/10/2010

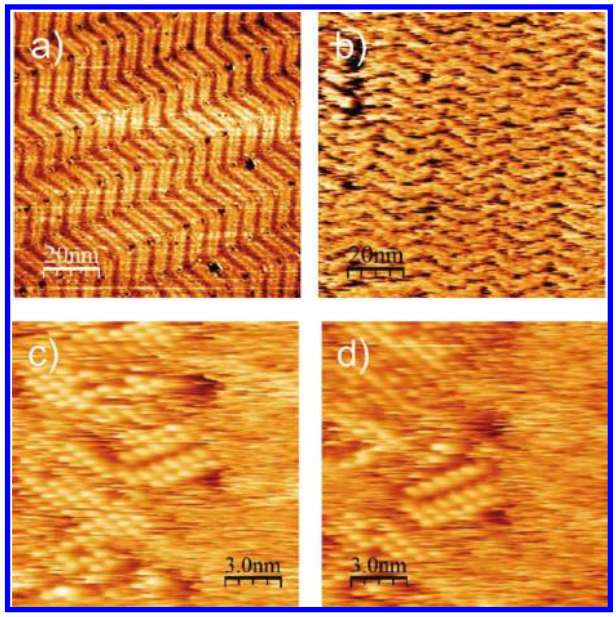

Figure 2. STM images of the Au surface during the very early stages of deposition. (a) Taken at 220 K; $\Theta < 0.1$ ML. (b−d) Consecutive images of the same region were taken at 160 K; $\Theta \sim 0.1$ ML. (a) $I = 0.49$ nA, $V_b = 1.486$ V; (b) $I = 0.24$ nA, $V_b = 1.25$ V; (c,d) $I = 0.10$ nA, $V_b = 1.25$ V.

the surface strongly depends on the intermolecular interactions and on the molecule−substrate interaction, the control of the morphology at the lateral scale requires the understanding of the individual interactions of each type of molecule with the gold substrate. Here we report a combined theoretical and experimental study on the self-assembly properties of exTTF on Au(111); a similar study for PCBM on Au(111) has already been published.[16]

exTTF is one of the most important derivatives of the parent tetrathiafulvalene (TTF).[17] The successive discoveries of high-electrical conductivity,[18] metallic behavior,[19] and superconductivity[20] in salts and charge-transfer complexes of TTF motivated the synthesis of new derivatives,[21−24] an investigation that was further stimulated by their possible application in organic solar cells as the electron donor material.[25]

Although many studies have focused on the self-assembly properties of organic molecules with good donor or acceptor properties,[16,26−34] only a few of them have been devoted to the adsorption of TTF and/or its derivatives on metal surfaces.[27−29] Reference 27 reported on the self-assembly of some relatively complex TTF derivatives at the interface between organic solutions and the graphite surface. In all cases where self-assembly was observed, the π-face of TTF was parallel to the surface. More related to our work, the adsorption of TTF on Au(111) has recently been studied both theoretical and experimentally.[28,29] The molecule−substrate interaction seems to be driven by the S−Au bonds, and a flat configuration has been predicted with the plane of the molecule parallel to the gold surface. Actually, the more sophisticated (DFT) calculation[29] predicted an asymmetric configuration (due to the incommensurate dimensions of molecule and surface lattice), where the plane of the molecule is slightly tilted (8°) with respect to the gold surface. There is a sizable (~0.6 e) charge donation from the molecule to the substrate with an adsorption energy of 0.86 eV per molecule.

Figure 1 displays the gas-phase conformation of exTTF, the minimum energy configuration corresponding to a butterfly shaped nonplanar structure.[35] The planar conformation of the

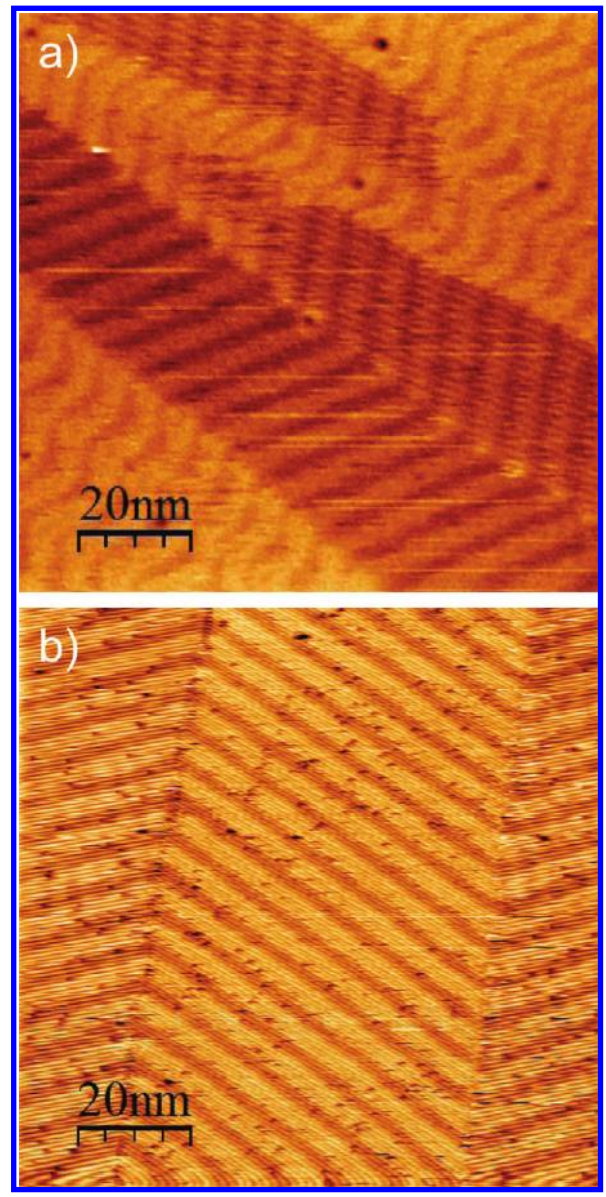

Figure 3. STM images of the Au surface after depositing (a) 0.5 ML ($I = 0.32$ nA, $V_b = 0.38$ V); (b) 1.0 ML ($I = 0.67$ nA, $V_b = -1.24$ V) of exTTF at room temperature. The darker areas in (a) are the exTTF islands. In (b) two domain boundaries are clearly seen. The images were taken with the sample at room temperature.

molecule is strongly hindered by the very short contacts between the sulfur atoms and the hydrogen atoms in peri positions. The main purpose of this work is to find out the adsorption configuration of this molecule on Au(111) since, as compared with TTF, it is not possible to have the four S atoms in close contact with the surface due to the distortion of the exTTF molecule out of planarity.

Figure 1 also shows a constant charge density surface colored according to the electrostatic potential. It can be seen that both the S atoms and the inside C atoms of central carbon rings show a slight negative charge. The nonplanar shape places this charge in an asymmetric way, creating an electric dipole of 2.23 D oriented perpendicular to the central C ring.

Experimental and Computational Methods

The growth of the molecular films and the STM measurements were carried out in an ultrahigh vacuum (UHV) chamber with a base pressure of $<2 \times 10^{-10}$ Torr, equipped with standard

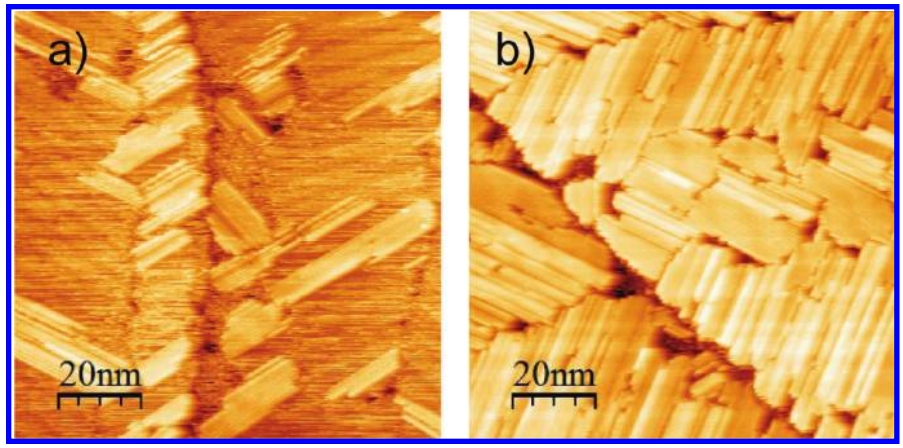

Figure 4. STM images of the Au surface after depositing (a) 1.2 ML ($I = 0.19$ nA, $V_b = -0.88$ V); (b) 2.1 ML ($I = 0.16$ nA, $V_b = -1.47$ V) of exTTF at room temperature. The images were taken with the sample at room temperature.

facilities for metal surface preparation, several low-temperature effusion cells and an Aarhus-type variable-temperature (down to 85 K) fast-scanning STM purchased from SPECS.

Photoemission measurements were performed in a separate UHV chamber located at the PM4 beamline in the Bessy II storage ring. This beamline is equipped with a plane grating monochromator and the SurICat end-station. The UHV system consisted of a sample preparation chamber interconnected to the analysis chamber. The spectra were taken by using a hemispherical electron energy analyzer (Scienta SES 100) with 120 meV energy resolution at 20 eV pass energy. The photon energy was set at 400 eV for the C 1s spectra and to 220 eV for the S 2p spectra.

Atomically flat, crystalline Au(111) surfaces were prepared by standard sputter/anneal procedures (sputter with 1 kV Ar^+ ions for 15 min followed by annealing to 800 K for another 15 min), which resulted in large terraces (about 200 nm wide), separated by monatomic steps. In both chambers the molecules were deposited from the same low-temperature Knudsen cell, heated at 400 K (well below the reported decomposition temperature, ~590 K[17]), onto the clean Au(111) substrate, which was held at room temperature. The deposition rate was calibrated by measuring the fraction of covered surface in large-area STM images. For the XPS experiments, coverages were deduced from the evaporation time and cross-checked by measuring the evolution of the areas of the C, S, and Au photoemission peaks. Considering the uncertainties involved, the error in this case has been estimated to be around 25%. STM measurements were carried out at room temperature and at low temperature (down to 140 K). Tunnelling conditions were chosen so as not to disturb individual molecules ($|V_b| > 1$ V, $I < 100-500$ pA). STM images were analyzed using the WSxM software.[36]

The DFT computations were performed using the VASP package.[37,38] The Perdew and Wang (PW91)[39] functional was adopted for electron−electron exchange and correlation interactions within the generalized gradient approximation (GGA). The projector augmented wave (PAW)[40,41] method was applied to describe ionic cores. The energy cutoff for the basis set was set at 280.0 eV, as dictated by the pseudopotential for sulfur. A four-layer gold slab was used to simulate the substrate, and the thickness of the vacuum above was about 12 atomic layers. Because of the large size of the chosen unit cells (see below), k-point sampling of the Brillouin zone during geometry optimization was restricted to the Γ-point only, with a Methfessel-Paxton smearing[42] of 0.2 eV. The adsorption was modeled by placing one exTTF molecule in the vacuum region of the supercell. For such a large molecule, it is virtually impossible to explore all possible configurations, so we only retained those that were compatible with the experimental data. As a matter of fact, for monolayer completion the packing is so close that the amount of degrees of freedom is strongly reduced, and the molecules have only two options, either stand upward interacting via H-atoms with the substrate, or to bend in a chairlike conformation to maximize the number of S−Au bonds, which turns out to be a much more stable configuration. The atomic positions of the whole exTTF molecule and the top two gold layers were then allowed to relax. The adsorption energy of the final structure (as given by the difference between the energy of the combined system and the sum of energies of a clean four-layer gold slab (with the top two layers relaxed) and an isolated exTTF molecule relaxed in the vacuum) was calculated using a $4 \times 4 \times 1$ sampling of the Brillouin zone.

Results and Discussion

After room temperature deposition, no isolated exTTF molecule could be imaged with the STM on the Au(111) surface, even at 140 K, possibly due to a high molecular diffusivity. Figure 2a shows a typical STM image taken during the very early stages of growth. The gold surface reconstruction is clearly visible, although it seems somewhat "blurred", due to the presence of diffusing molecules over the surface, which may also be the origin of the horizontal white lines in the image. The elbows of the reconstruction look darker, when compared with the clean surface, maybe due to a longer residence time of the molecules in these preferential nucleation sites. When increasing the coverage (Figure 2b), the reconstruction becomes even more diffuse. At this point some small islands start to form, although they are not completely stable; molecules are continuously attaching and detaching from the islands, as can be seen in Figure 2c,d, taken at 160 K, where two consecutive images of the same area of the surface are shown.

Upon increasing the coverage, stable islands start to form (Figure 3a). These islands are strongly elongated with their long side parallel to the lines joining the elbows of the herringbone reconstruction. The edges of the islands do not look sharp and the space between the islands still appears diffuse, which seems to be an indication of the coexistence of a 2D lattice gas of molecules in equilibrium with the condensed phase.[43] The gold reconstruction is still visible under the molecular layer, although the geometry is slightly different when compared to the clean gold surface (see below). The minimum observed width of a

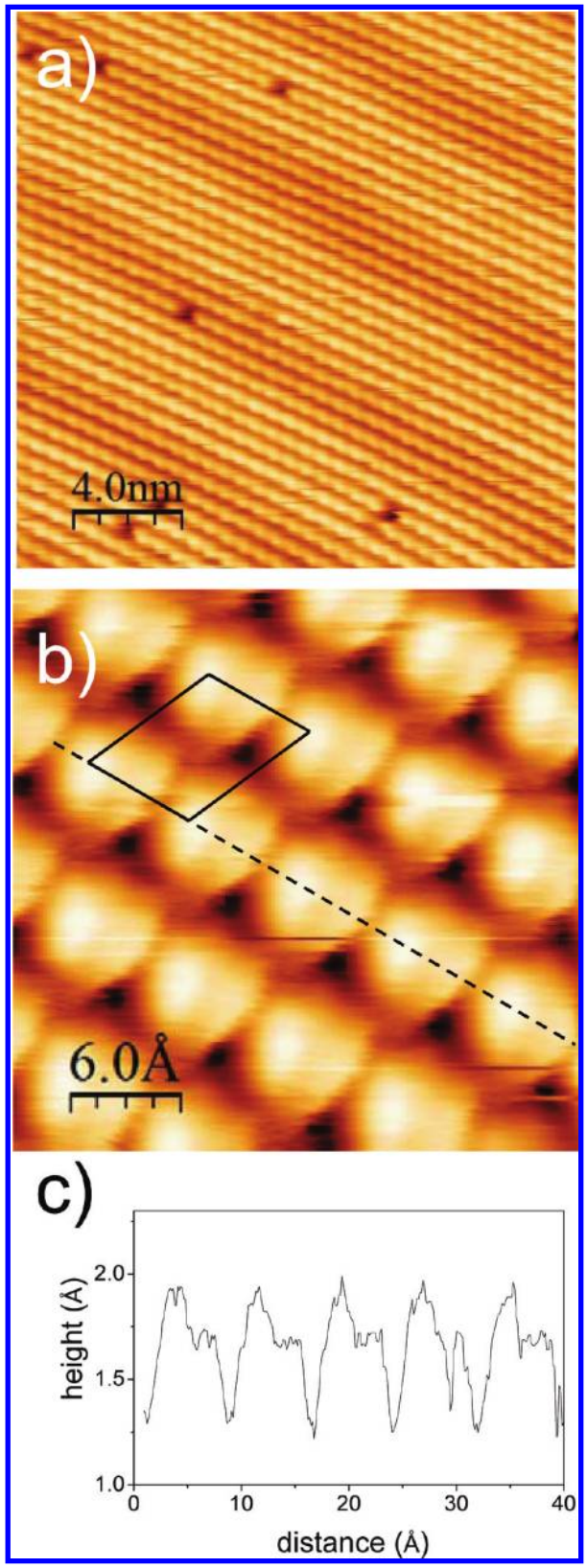

Figure 5. (a,b) Close-up STM images of the internal island structure (a) $I = 0.45$ nA, $V_b = 1.24$ V; (b) $I = 1.11$ nA, $V_b = 1.24$ V). The solid line in (b) marks the rhombohedral unit cell. (c) Height profiles along the dashed lines drawn in (b).

stable island is around ~200 Å, and it increases with coverage up to ~700 Å, when the islands coalesce and the first monolayer is complete (Figure 3b). Only at this moment a second monolayer starts to grow (Figure 4a), which might also indicate a high diffusivity of the exTTF molecules on top of the first exTTF monolayer. As a consequence, second-layer islands start to nucleate at the domain boundaries of the first layer (Figure 4a) and continue to grow in a two-dimensional way (Figure 4b).

Higher resolution images (Figure 5a) show that the first layer islands are composed of rows of molecules, which have an angle of 10° with the reconstruction lines of the gold surface. A further close up (Figure 5b) reveals the molecular structure of the islands. The unit cell of the exTTF monolayer (drawn in solid black in Figure 5b) is rhombohedral with sides ~10.3 and ~7.7 Å long, which form an angle of 65° between them. These measurements are compatible with a commensurate structure that in standard matrix notation can be described as

$$\begin{bmatrix} 4 & 1 \\ 2 & 3 \end{bmatrix}$$

relative to the crystallographic directions of the gold surface (see Figure 6a).

To find out the adsorption conformation, DFT calculations were performed both for an "isolated" molecule (using a (5 × 5) supercell containing 100 gold atoms) on an hexagonal unreconstructed Au(111) surface, and for a complete exTTF monolayer (using the experimentally measured unit cell)

$$\begin{bmatrix} 4 & 1 \\ 2 & 3 \end{bmatrix}$$

with very similar results. As shown in Figure 7, the molecule adopts a butterfly conformation, very similar to the one found in gas phase. As in TTF, the bond to the surface is dominated by the sulfur atoms. In this case, however, and due to geometry restrictions, the four sulfur atoms cannot be bonded to the surface simultaneously. Instead, only one of the two dithiole rings is close and almost parallel to the surface, while the other is almost perpendicular to it. The S atoms tend to be close to on-top positions of the substrate with the average distance to the surface being around 3.0 Å. At the same time, the Au atoms directly below are slightly pulled-up (~0.1 Å). The calculated adsorption energy is 0.32 eV per exTTF molecule, which is ~0.1 eV smaller than half the adsorption energy of TTF on Au(111) (0.86 eV).

Figure 8 shows a comparison between the calculated and an experimental STM image taken at a bias voltage $V_b = -2.0$ V. Although the molecular appearance is strongly dependent on the tunneling and tip conditions, in general the molecular shape is rather irregular, displaying only mirror symmetry along one axis running parallel to the molecular rows (Figure 5b and Figure 8). Along this line two nonequivalent maxima, separated ~3 Å, are visible, as shown by the line profile in Figure 5c. The agreement with the theoretical calculation, which shows clearly the origin of these two maxima, is rather good. Also visible in both cases are the side-wings features corresponding to the external C rings.

The predicted theoretical conformation of the exTTF molecule on Au(111) is supported by photoemission (XPS) experiments. Figure 9 shows the S 2p spectrum for two different coverages. Due to the spin−orbit splitting effect, the S 2p spectra are composed of $2p_{3/2}$ and $2p_{1/2}$ peaks separated 1.2 eV and with an intensity ratio of 2:1. For submonolayer coverages the measured spectrum consists of two doublets with S $2p_{3/2}$ binding energies of 163.52 and 164.03 eV, respectively, which indicates the existence of two different types of sulfur atoms. Besides, the intensity ratio of these two peaks is close to 1 (between 0.8 and 0.9). The higher binding energy component is probably due to the two sulfur atoms not directly interacting with the substrate,

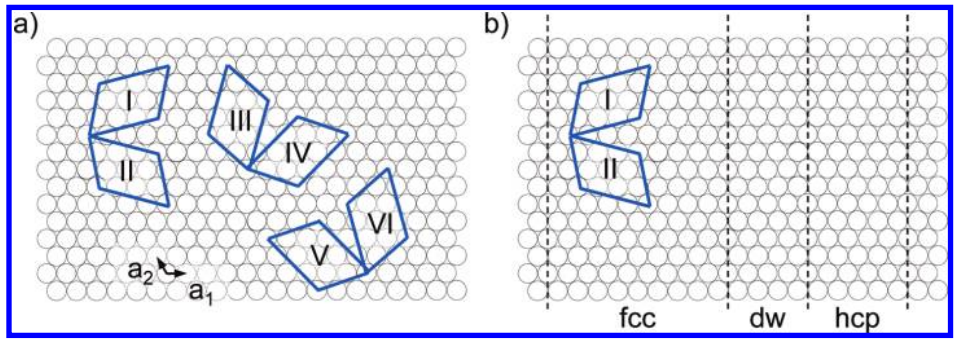

Figure 6. (a) The six possible orientations of the experimentally measured rhombohedral unit cell on an unreconstructed hexagonal surface. (b) Experimentally, however, for a given direction of the Au(111) surface reconstruction, only two domains are observed. If, for example, the domain walls run parallel to the dashed lines drawn in the figure, only domains I and II are present.

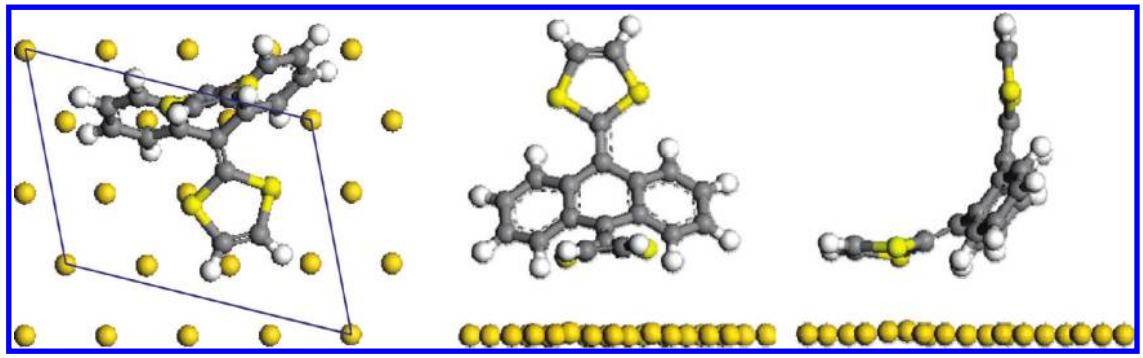

Figure 7. Top, front, and side view of the calculated minimum energy conformation for an exTTF molecule on the Au(111) unreconstructed surface. The solid line represents the unit cell of the complete monolayer.

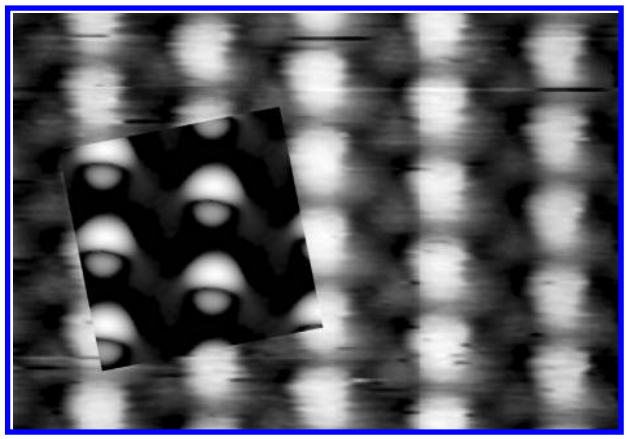

Figure 8. Comparison between the calculated STM image and the experimental one at $V_b = -2.0$ V.

because the photoemission-induced core holes are not well screened by the valence electrons of the substrate, while the low-binding energy component is due to the sulfur atoms close to the surface. In accordance with this interpretation, for coverages beyond the monolayer the relative intensity of this low energy peak decreases, since the interaction of second layer molecules with the substrate surface is much smaller. The measured binding energies are compatible with those reported for other weakly adsorbed S-containing adsorbates, while for chemisorbed systems it is significantly lower.[44]

The interpretation of the C peak is more complicated, due to the larger number of different types of C atoms (there are at least five different C atoms in the gas phase molecule). However, the fact that the peak shape does not change with the coverage indicates that the C atoms are not very sensitive to the presence of the surface, which is consistent with the molecule being bound to the substrate mainly through the S atoms.

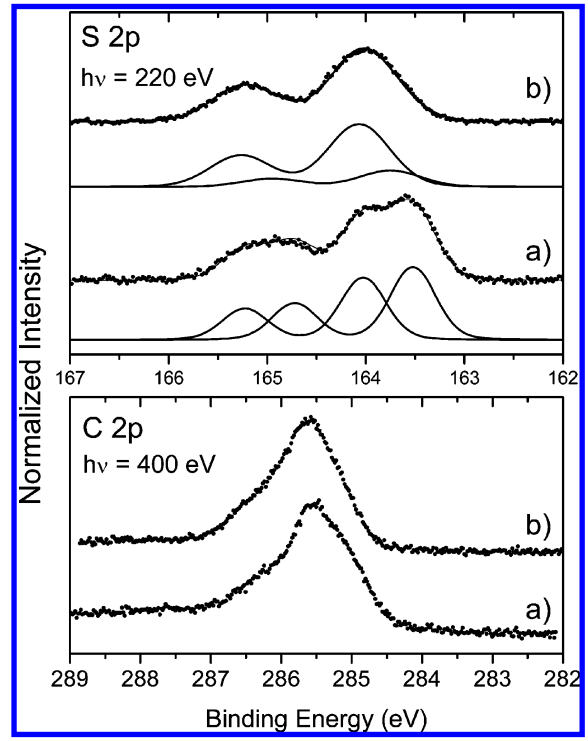

Figure 9. S 2p and C 2p core levels measured after depositing (a) 0.5 ML; (b) 2 ML of exTTF on Au(111). The spectra have been normalized to the same intensity. The continuous line in the top panel show the fit to the experimental data points and the corresponding decomposition into doubles for the S 2p core level.

The bottom panel in Figure 10 shows the valence band spectra measured by ultraviolet photoemission spectroscopy for different exTTF coverages. The lowest spectra, Figure 10a, corresponds to the clean Au(111) surface. After depositing a small amount

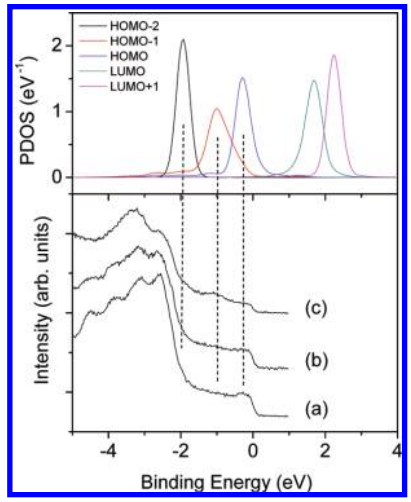

Figure 10. Bottom: Valence band spectra measured after depositing (b) 0.5 ML; (c) 2 ML of exTTF on (a) the clean Au(111) surface. Top: Calculated projected density of states for 1 ML of exTTF on Au(111).

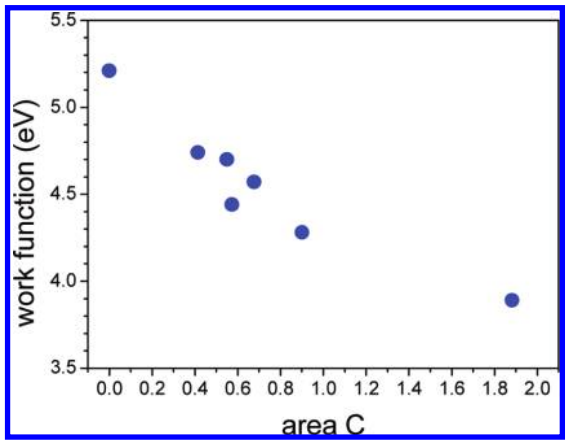

Figure 11. Evolution of the experimentally measured work function with coverage.

of exTTF (~0.5 ML), the intensity of the Au related features decreases appreciably, but no exTTF-related new structure is clearly discernible (Figure 10b). These become more noticeable (at −0.2, −1.0, and −2.0 eV) after depositing ~2 ML of exTTF (Figure 10c). The theoretical density of states projected onto the molecular orbitals is also shown (top panel). As can be seen, the experimental features correspond quite well to the calculated positions of the HOMO, HOMO-1, and HOMO-2, respectively. On the other hand, the energies of the corresponding orbitals for exTTF molecules in the gas phase are −4.16, −4.78, −5.97 eV, which are close to the experimental values found for the molecular overlayer if a rigid shift of ~3.8 eV (that is, the experimental work function of the system exTTF/Au(111), see below and Figure 11) is assumed. In conclusion, the gas-phase molecular orbitals are little affected by the adsorption on the Au(111) surface; the main effect is a partial charge transfer from the molecule to the substrate, which causes the HOMO to be partially empty (as can be seen in the top panel of Figure 10). The estimated charge transfer is ~0.3 e per molecule, which is about half the value reported for TTF on Au(111).[29]

A partial charge transfer from the molecule to the substrate is also supported by the decrease of the work function while increasing the amount of exTTF coverage (Figure 11). From the total change ($\Delta W \sim -1.3$ eV), one can obtain the change of the surface dipole upon adsorption, $\Delta\mu = \varepsilon_0 A \Delta W/e$, where

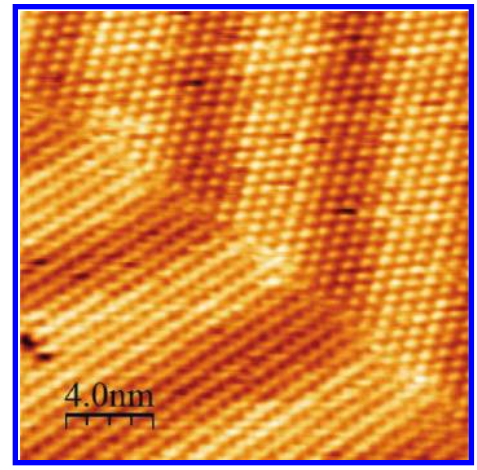

Figure 12. Domain wall between two molecular domains.

ε_0 is the permittivity of vacuum and A is the area of the surface unit cell (since the unit cell contains one molecule, $\Delta\mu$ is the change in the surface dipole per adsorbed molecule). The result gives $\Delta\mu = -1.91$ D, that is, the surface dipole decreases upon exTTF adsorption. Part of this decrease is due to the electrostatic dipole of the exTTF molecule, which in the gas-phase configuration amounts to 2.23 D. Taking into account the adsorption geometry (Figure 7), its projection along the surface normal would give $\Delta\mu = -1.57$ D, since the dipole is pointing outward the surface (i.e., opposite to the metal dipole layer). The small difference with the experimentally measured value is probably due to the charge transfer from the molecule to the substrate, which causes an additional decrease of the total surface dipole layer.

In the above considerations no attention has been paid to the reconstruction of the Au(111) gold surface and its influence on the arrangement of the exTTF overlayer. On an unreconstructed hexagonal lattice there are six symmetry-related possible orientations of a rhombohedral unit cell (Figure 6a), which should give rise to six different molecular domains. All of them can be found in the exTTF layer in different regions of the sample surface, but in every case the orientation of the molecular domains is strongly determined by the direction of the underlying surface reconstruction. As can be seen in Figure 12, the overlayer unit cell changes its direction in accordance with the direction of the surface reconstruction, in such a way that the short side always has an angle of ±10° with the domain walls direction. Thus, the small structural differences between the different orientations produced by the anisotropic compression of the gold surface cause that, for a given direction of the surface reconstruction, only two domains are observed (domains I and II in Figure 6b). A similar influence of the Au(111) surface reconstruction on the orientation of other adsorbed molecular systems (methanethiol,[45] bipyridine[46]) on Au(111) has been previously reported. The effect has been attributed[45] to an anisotropic mass transport on the surface due to the herringbone reconstruction, that is, it was concluded that for the preferred molecular orientation the "leaky" domain walls of the molecular overlayer (those domain walls were the probability of molecular detachment are greater) should run parallel to the domain walls of the surface reconstruction, where the binding energy is lower. This would reduce the rate of molecular detachment, making these domains to grow faster than the other domains. However, preliminary results seem to indicate that, for exTTF on Au(111), surface diffusion is indeed anisotropic, but the direction of fast diffusion is parallel to the short side of the unit cell, which makes the "leaky" edges perpendicular to the surface domain walls,

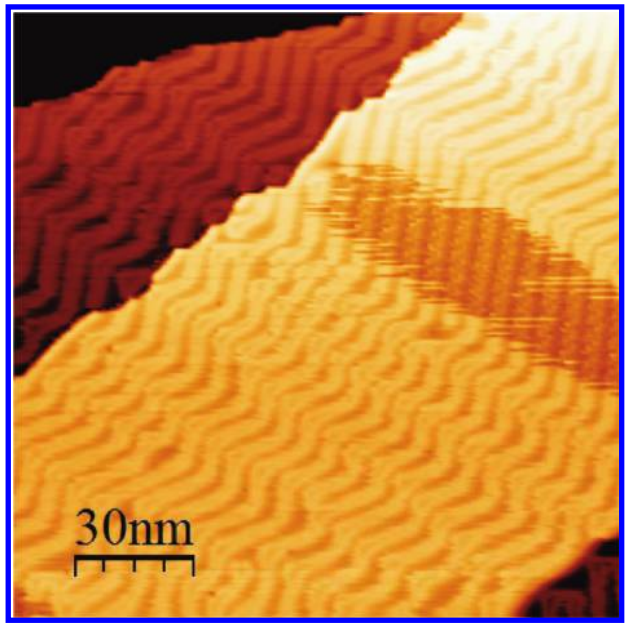

Figure 13. STM image of a partially covered gold surface; $\Theta \approx 0.2$ ML. ($I = -0.49$ nA, $V_b = -1.16$ V).

in opposition to the explanation suggested in ref 45. We do not have at present an explanation for the dominance of just one type of domain, but current studies are under way to dilucidate if the origin is kinetic or thermodynamics.

Reciprocally, if the surface reconstruction has a clear effect on the arrangement of the exTTF molecules, the molecule−substrate interaction is large enough to cause alterations in the geometric structure of the herringbone reconstruction. The periodicity of the gold reconstruction below the exTTF overlayer is $\sim 72.7 \pm 1.5$ Å, instead of the $\sim 60.9 \pm 3.1$ Å observed for the clean Au surface.[47] This means that now there is one extra atom in the surface layer every 25 (or 26) atoms in the bulk, instead of every 22 atoms as in the clean surface. In addition, the STM images (Figure 13) seem to indicate that the hcp areas disappear, remaining only areas with fcc stacking and domain walls. The width of the molecular domains also increases and the reconstruction changes orientation every ~700 Å, instead of every ~250 Å as in the case of the clean surface. This is, thus, an intermediate situation between molecular systems that have little or no influence on the herringbone reconstruction, and those where it is completely lifted.

Conclusions

In summary, as in the case of TTF on Au(111), the interaction of exTTF with the gold surface is dominated by the S−Au bonds. The molecule adopts a conformation very similar to the gas-phase conformation with the two dithiole rings almost perpendicular to each other, and only one in close contact with the gold surface. That is, in this case and due to geometric reasons, there are only two sulfur atoms strongly interacting with the surface, instead of four, which makes the interaction strength (as measured by the adsorption energy or the charge transfer with the substrate) significantly smaller (less than half) than for TTF. Nevertheless, this seems to be enough to cause distortions in the geometry of the gold herringbone reconstruction, probably due to the partial charge transfer (0.3 e per molecule) from exTTF to the susbstrate.

This results provide a hint about how to tune-up the interaction of other exTTF derivatives with the Au(111) surface, as long as the number of in-plane sulfur atoms can be controlled.

Acknowledgment. We acknowledge financial support from the Spanish MICINN (Project NAN2004-08881-C02-01, Project FIS2007-61114, Project FIS2007-66711-C02-01, Project FIS2007-60064, Project MAT2007-66719-C03-03, Project CT2008-00795/BQU, Project CONSOLIDER-INGENIO EN NANOCIENCIA MOLECULAR ref CSD2007-00010, and Project CONSOLIDER-INGENIO FUNCOAT ref CSD2008-00023), from the Comunidad de Madrid (Project GR/MAT/0435/2004, Project P-PPQ-000225-0505, and Project S-0505/MAT/0194), and from GV-UPV/EHU (grant IT-366-07). We also thank the CCC-UAM and BSC for allocation of computer time.

References and Notes

(1) Witte, G; Wöll, Ch. *Phys. Status Solidi A* **2008**, *205*, 497.
(2) Dimitrakopoulos, C. D.; Malenfant, P. R. L. *Adv. Mater.* **2002**, *14*, 99.
(3) Koch, N. *J. Phys.: Condens. Matter* **2008**, *20*, 184008.
(4) Braun, S.; Salaneck, W. R.; Fahlman, M. *Adv. Mater.* **2009**, *21*, 1450.
(5) Reese, C.; Roberts, M.; Ling, M.; Bao, Z. *Mater. Today* **2004**, *7*, 9–20.
(6) Sariciftci, N. S. *Mater. Today* **2004**, *7*, 9–36.
(7) Borchardt, J. K. *Mater. Today* **2004**, *7*, 9–42.
(8) Halls, J. J. M.; Walsh, C. A.; Greenham, N. C.; Marseglia, E. A.; Friend, R. H.; Morati, S. C.; Holmes, A. B. *Nature* **1995**, *376*, 498.
(9) Yu, G.; Gao, J.; Hummelen, J. C.; Wudl, F.; Heeger, A. J. *Science* **1995**, *270*, 1789.
(10) Hoppe, H.; Niggemann, M.; Winder, C.; Kraut, J.; Hiesgen, R.; Hinsch, A.; Meissner, D.; Sariciftci, N. S. *Adv. Funct. Mater.* **2004**, *14*, 1005.
(11) Otero, R.; Écija, D.; Fernández, G.; Gallego, J. M.; Sánchez, L.; Martín, N.; Miranda, R. *Nano Lett.* **2007**, *7*, 2602.
(12) Wang, L.; Chen, Q.; Pan, G.; Wan, L.; Zhang, S.; Zhan, X.; Northrop, B. H.; Stang, P. J. *J. Am. Chem. Soc.* **2008**, *130*, 13433.
(13) Chen, W.; Zhang, H. L.; Huang, H.; Chen, L.; Wee, A. T. S. *Appl. Phys. Lett.* **2008**, *92*, 193301.
(14) Nelson, J. *Curr. Opin. Solid State Mater. Sci.* **2002**, *6*, 87.
(15) Sylvester-Hvid, K. L.; Rettrup, S.; Ratner, M. A. *J. Phys. Chem. B* **2004**, *108*, 4296.
(16) Écija, D.; Otero, R.; Sánchez, L.; Gallego, J. M.; Wang, Y.; Alcamí, M.; Martín, F.; Martín, N.; Miranda, R. *Angew. Chem., Int. Ed.* **2007**, *46*, 7844.
(17) Yamashita, Y.; Kobayashi, Y.; Miyashi, T. *Angew. Chem., Int. Ed. Engl.* **1989**, *28*, 1052.
(18) Wudl, F.; Wobschall, D.; Hufnagel, E. J. *J. Am. Chem. Soc.* **1972**, *94*, 670.
(19) Ferraris, j.; Cowan, D. O.; Walatka, V. V.; Perlstein, J. H. *J. Am. Chem. Soc.* **1973**, *95*, 948.
(20) Parkin, S. S. P.; Engles, E. M.; Schumaker, R. R.; Lagier, R.; Lee, V. Y.; Scott, J. C.; Greene, R. L. *Phys. Rev. Lett.* **1983**, *50*, 270.
(21) Bryce, M. R. *Adv. Mater.* **1999**, *11*, 11.
(22) Segura, J. L.; Martín, N. *Angew. Chem., Int. Ed.* **2001**, *40*, 1372.
(23) Bendikov, M.; Wudl, F.; Perepichka, D. F. *Chem. Rev.* **2004**, *104*, 4891.
(24) Canevet, D.; Sallé, M.; Zhang, G.; Zhang, D.; Zhu, D. *Chem. Commun.* **2009**, 2245.
(25) Martín, N.; Sánchez, L.; Herranz, M. A.; Illescas, B.; Guldi, D. M. *Acc. Chem. Res.* **2007**, *40*, 1015.
(26) Kamma, M. M.; Graham, T. M.; Love, J. C.; Weiss, P. S. *Surf. Sci.* **1998**, *419*, 12.
(27) Adbel-Mottaleb, M. M. S.; Gomar-Nadal, E.; Surin, M.; Uji-i, H.; Mamdouh, W.; Veciana, J.; Lemaur, V.; Rovira, C.; Cornil, J.; Lazzaroni, R.; Amabilino, D. B.; De Feyter, S.; De Schryver, F. C. *J. Mater. Chem.* **2005**, *15*, 4601.
(28) Fueno, H.; Hayashi, M.; Nin, K.; Kubo, A.; Misaki, Y.; Tanaka, K. *Curr. Appl. Phys.* **2006**, *6*, 939.
(29) Fernández-Torrente, I.; Monturet, S.; Franke, K. J.; Fraxedas, J.; Lorente, N.; Pascual, J. I. *Phys. Rev. Lett.* **2007**, *99*, 176103.
(30) Gomar-Nada, E.; Puigmartí-Luis, J.; Amabilino, D. B. *Chem. Soc. Rev.* **2008**, *37*, 490.
(31) Wegner, D.; Yamachika, R.; Wang, Y.; Brar, V. W.; Bartlett, B. M.; Long, J. R.; Crommie, M. *Nano Lett.* **2008**, *8*, 131.
(32) Jäckel, F.; Perera, U. G. E.; Iancu, V.; Braun, K. F.; Koch, N.; Rabe, J. P.; Hla, S. W. *Phys. Rev. Lett.* **2008**, *100*, 126102.
(33) Fernández-Torrente, I.; Franke, K. J.; Pascual, J. I. *Int. J. Mass. Spectrosc.* **2008**, *277*, 269.

(34) Gonzalez-Lakunza, N.; Fernández-Torrente, I.; Franke, K. J.; Lorente, N.; Arnau, A.; Pascual, J. I. *Phys. Rev. Lett.* **2008**, *100*, 156805.
(35) Martín, N.; Sánchez, L.; Seoane, C.; Ortí, E.; Viruela, P. M.; Viruela, R. *J. Org. Chem.* **1998**, *63*, 1268.
(36) Horcas, I.; Fernández, R.; Gómez-Rodríguez, J. M.; Colchero, J.; Gómez-Herrero, J.; Baró, A. M. *Rev. Sci. Instrum.* **2007**, *78*, 013705.
(37) Kresse, G.; Hafner, J. *Phys. Rev. B* **1993**, *47*, 558.
(38) Kresse, G.; Furthmüller, J. *Comput. Mater. Sci.* **1996**, *6*, 15.
(39) Perdew, J. B.; Wang, Y. *Phys. Rev. B* **1992**, *45*, 13244.
(40) Blöchl, P. E. *Phys. Rev. B* **1994**, *50*, 17953.
(41) Kresse, G.; Joubert, D. *Phys. Rev. B* **1999**, *59*, 1758.
(42) Methfessel, A.; Paxton, A. T. *Phys. Rev. B* **1989**, *40*, 3616.
(43) Berner, S.; Brunner, M.; Ramoino, L.; Suzuki, H.; Güntherodt, H. J.; Jung, T. A. *Chem. Phys. Lett.* **2001**, *348*, 175.
(44) Vericat, C.; Vela, M. E.; Andreasen, G.; Salvarezza, R. C.; Vázquez, L.; Martín-Gago, J. A. *Langmuir* **2001**, *17*, 4919.
(45) Maksymovych, P.; Dougherty, D. B. *Surf. Sci.* **2008**, *602*, 2017.
(46) Dretschkow, Th.; Lampner, D.; Wandlowski, Th. *J. Electroanal. Chem.* **1998**, *458*, 121.
(47) Harten, U.; Lahee, A. M.; Toennies, J. P.; Wöll, Ch. *Phys. Rev. Lett.* **1985**, *54*, 2619.

JP911839B